Mon. Not. R. Astron. Soc. **357,** L26–L30 (2005) doi:10.1111/j.1745-3933.2005.08638.x

Adaptive optics for high-contrast imaging: pyramid sensor versus spatially filtered Shack–Hartmann sensor

C. Vérinaud,[1]★ M. Le Louarn,[1] V. Korkiakoski[1] and M. Carbillet[2]

[1]*European Southern Observatory, Karl-Schwarzschild-str 2, 85748 Garching bei München, Germany*
[2]*Laboratoire Universitaire d'Astrophysique de Nice, UMR 6525, Parc Valrose, 06108 Nice Cedex 02, France*

Accepted 2004 November 10. Received 2004 October 9; in original form 2004 August 19

ABSTRACT

A comparison between pyramid-based and spatially filtered Shack–Hartmann-based high-order adaptive optics (AO) is presented in the framework of 8-m-class and extremely large telescopes (ELTs). We first show, with end-to-end simulations of an 8-m AO assisted telescope, how each sensor deals with the aliasing error, which may be the dominant error source at high flux. Then, focusing on photon noise error propagation, we study the field dependence of the sensitivity gain provided by the pyramid sensor with respect to the Shack–Hartmann sensor. From this analysis, we investigate, with an analytical model, visible correction on ELTs for detection of Earth-like exoplanets.

Key words: instrumentation: adaptive optics – techniques: high angular resolution – planetary systems.

1 INTRODUCTION

The direct detection of exoplanets, with the ultimate goal of finding evidence of biological activity, is one of the major challenges of the 21st century. Angel (1994), in his study of direct exoplanet detection with adaptive optics (AO), has already emphasized the central role that the wavefront sensor plays. In the present study, we compare the spatially filtered Shack–Hartmann sensor (Poyneer & Machintosh 2004) and the pyramid sensor (Ragazzoni 1996) that have been proposed for the AO system of the European Southern Observatory Planet Finder (PF) project for the Very Large Telescope (Beuzit et al. 2004; Berton et al. 2004). For the comparison, we concentrate on the fundamental behaviours of the sensors in the Fourier domain. In Section 2, we briefly present, for each sensor, the two main error sources affecting the wavefront measurements, namely aliasing and photon noise. In Section 3, a comparison by means of end-to-end simulations of PF-like systems in the high-flux regime shows how aliasing is handled by each sensor. Then, in Section 4, we discuss, using mainly analytical methods, the very different behaviours of the sensors with respect to photon noise. We then investigate the astrophysical implications in the perspective of visible light AO correction with natural guide stars on extremely large telescopes (ELTs) for detection and characterization of Earth-like exoplanets.

2 BASIC PROPERTIES OF THE SENSORS

Throughout this study, we use the property that the corrected phase power spectrum density (PSD) $\langle|\tilde{\phi}(f)|^2\rangle$, where $\tilde{\phi}(f)$ is the Fourier transform of the wavefront phase ϕ and $\langle\,\rangle$ denotes temporal averaging, is a good approximation of the image halo (Jolissaint & Véran 2002) at the angular position $\lambda_{\rm obs}f$, where f is the spatial frequency and $\lambda_{\rm obs}$ the imaging wavelength. We consider monodimensional PSDs of the residual phase, and assume as a useful simplification that the real PSDs are radially symmetric.

The Shack–Hartmann (SH) sensor is one of the most popular sensors in AO for astronomy. Geometrical optics show that it measures the average slopes of the wavefront over individual sub-apertures. A Fourier analysis (Rigaut, Véran & Lai 1998) shows that the photon noise propagation PSD on the range $[F_0, F_{\rm c}]$ is proportional to $d^{-2}f^{-2} \times \mathrm{sinc}^{-2}(df)$ ($F_0 = 1/D$, with D the telescope diameter, is the smallest spatial frequency controlled by the AO system, and the highest $F_{\rm c} = 1/2d$, with d the sub-aperture size, is called the cut-off frequency). This property implies that low orders suffer much more from photon noise propagation than high orders. A novel centroid estimator that will be considered in this study [hereafter weighted centre of gravity (WCOG) (Nicolle et al. 2004)], permits us to decrease significantly the error on the slopes: the authors have shown that multiplying each sub-aperture image (the full width at half-maximum of which is FWHM $= N_{\rm T}$ pixels) by a likelihood function (Gaussian for example) with FWHM $= N_{\rm W}$ decreases the photon noise error variance by a factor of $(2N_{\rm T}^2 + N_{\rm W}^2)^2/(N_{\rm T}^2 + N_{\rm W}^2)^2$. In the photon noise limited regime and for high correction, the maximum improvement is obtained for $N_{\rm W} = N_{\rm T}$, yielding thus a gain of 9/4 (0.88 mag). The second major result of the Fourier analysis is that aliasing affects all the frequencies down to F_0 and the PSD is slightly increasing until $F_{\rm c}$ where it reaches its maximum. To overcome this limitation, Poyneer & Machintosh (2004) proposed using a diaphragm of size $\lambda_{\rm wfs}/d$ in a focal plane before the SH sensor, where $\lambda_{\rm wfs}$ is the sensing wavelength. The effect is

★E-mail: cverinau@eso.org

clearly to filter out the high spatial content of the wavefront that is not corrected by the system. This spatially filtered SH (SFSH) sensor is thus able to attenuate dramatically the residual halo in the corrected images with respect to a conventional SH sensor.

The pyramid sensor (PS) is a more recent concept for wavefront sensing. Ragazzoni (1996) first described it by geometrical optics as a slope sensor. However, this model is only valid when a large dynamic beam modulation is applied. In fact, several peculiar behaviours of the PS in terms of error propagation can be better explained by a diffractive model (Vérinaud 2004). The latter shows that the PS is somewhat similar to a phase sensor, and predicts the following properties for the two main error sources in which we are interested. The PSD of the photon noise propagation is almost flat [$\propto f^0 \times \mathrm{sinc}^{-2}(df)$], with essentially the same signal-to-noise ratio (S/N) as the Mach–Zehnder-based direct phase sensor proposed by Angel (1994). Aliasing is almost negligible in the low-order part of the PSD and climbs very rapidly to the same amount as a SH sensor around F_c.

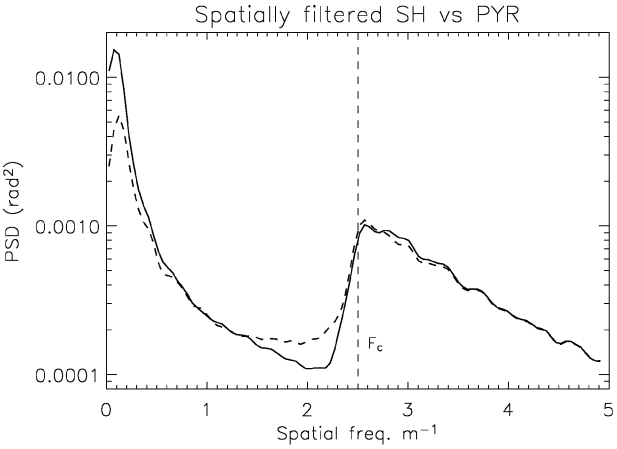

Figure 2. PSD of residuals for the SFSH sensor (filter size: $1.1\lambda/d$) (solid line) and the PS (dashed line). Seeing: 0.85 arcsec, high flux.

3 PERFORMANCE AT HIGH FLUX

In this section we compare, with end-to-end simulations (see description in Le Louarn et al. 2004; Korkiakoski, Vérinaud & Le Louarn 2004), the performance of the sensors on an 8-m telescope in the high-flux regime and for median-turbulence conditions (seeing: 0.85 arcsec at 500 nm; coherence time: $\tau_0 = 3$ ms). The main parameters of these PF-like systems are the following: the sub-aperture size is $d = 20$ cm (40×40) and 1000 Karhunen–Loeve modes are controlled at 2 kHz. The sensing wavelength is $\lambda_{\mathrm{wfs}} = 700$ nm.

We first concentrate on a SFSH sensor with 6×6 pixels per sub-aperture, sampling a 2.4-arcsec field of view, and we investigate the effect of the width of a square spatial filter in attenuating aliasing. The results in terms of the Strehl ratio (SR) and of the PSD are displayed in Fig. 1. The improvement of the SR in the K band is about 3 per cent for the three widths considered here. This small dispersion in SR is, however, not very representative of the real impact of the filter size on the performance. Indeed, as we can see in Fig. 1, the value of the PSD is reduced by nearly a factor of 10 with respect to a classical SH sensor, but only in a limited range of spatial frequencies, if the spatial filter is greater than λ_{wfs}/d. Hence the filter size should be kept as close as possible to λ_{wfs}/d to correct the largest possible field from aliasing, as long as it is compatible with AO loop stability (Korkiakoski et al. 2004).

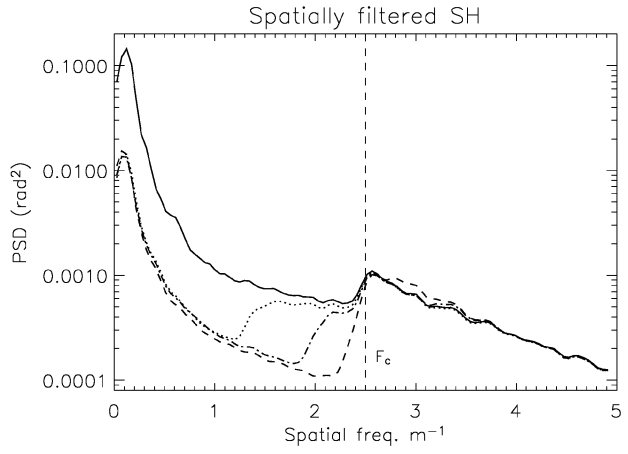

Figure 1. Circularly averaged PSD of residuals in K for different filter sizes of the SFSH sensor. Solid line: no spatial filter (SR = 0.931); dotted line: filter size is $1.5\lambda_{\mathrm{wfs}}/d$ (SR = 0.957); dot–dashed line: $1.25\lambda_{\mathrm{wfs}}/d$ (SR = 0.959); dashed line: $1.1\lambda_{\mathrm{wfs}}/d$ (SR = 0.960). Seeing: 0.85 arcsec, high flux.

Let us compare now the performance of a SFSH sensor with a $1.1\ \lambda_{\mathrm{wfs}}/d$ filter width and a PS. The results are very similar for both sensors (SR = 0.96). Again some differences can be noticed in the residual PSDs (see Fig. 2): the SFSH sensor shows somewhat more noise propagation for the very lowest orders; this has been identified as the effect of pupil intensity variations induced by the filter. At the edge of the corrected field, the SFSH sensor shows slightly better performance, since aliasing for the PS is still present near F_c (Vérinaud 2004).

4 IMPACT OF PHOTON NOISE

In fig. 7 of Vérinaud (2004), the photon noise propagation PSD for both sensors was compared in the case of diffraction-limited spots in the SH sub-apertures (a good hypothesis for small sub-apertures) and sampled by a quad-cell. In this case, at each spatial frequency, the SH noise propagation is higher than for the PS, except at F_c where they are equal. However, it is possible to decrease the noise in a SH sensor by increasing the number of pixels [if read-out noise is negligible, the gain is 2 ln2 (Fusco et al. 2004)], and by using the WCOG algorithm (a further gain of 9/4). In this case, the theoretical noise propagation PSD for the SFSH sensor is shifted downwards with respect to the quad-cell SH sensor by multiplying it by $(9/4 \times 2\ln(2))^{-1}$. As a consequence, less noise propagation for the SH sensor is expected for the highest frequencies and thus a better contrast than with a PS should be obtained towards the edge of the AO-corrected field when photon noise dominates. We have verified this by numerical simulations. We have simulated the 40×40 system with the PS and the SFSH sensor with the WCOG algorithm for a flux of 20 photons per sub-aperture and the same conditions as in Section 3. The overall gains have been optimized to maximize the SR (0.4 for the SFSH sensor and 0.6 for the PS). We have also run two other cases with classical centroiding, and in one of them we applied a factor of 9/4 to the number of photons reaching the SFSH sensor to mimic WCOG. The results are presented in Fig. 3 in terms of intensity in the halo (K band) obtained from the simulated PSDs scaled to the field: first, the gain brought by the WCOG is near but slightly less than the theoretical one since the N_{W} parameter needed to be adjusted, to avoid non-linearity, to a larger value than the

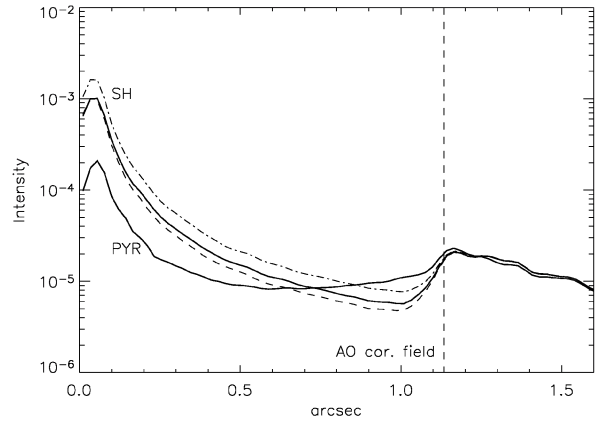

Figure 3. Circularly averaged residual halo (K band) (seeing: 0.85 arcsec, 20 photons per sub-aperture) for the SFSH with the WCOG algorithm (SR = 0.946) and the PS (SR = 0.955) (solid line); SFSH sensor without the WCOG, 20 photons per sub-aperture (dot–dashed line), 45 photons per sub-aperture (dashed line).

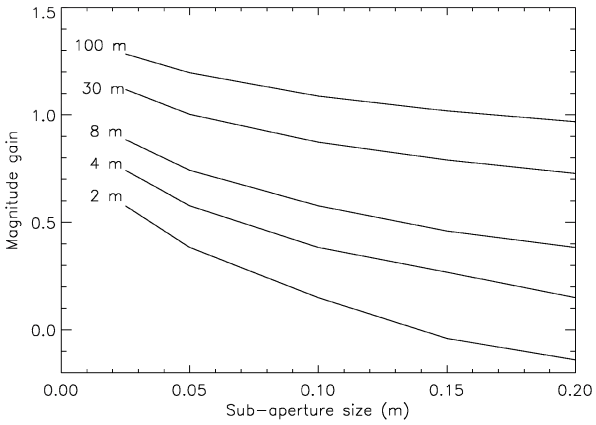

Figure 5. Gain in magnitude of the PS over the SH sensor in terms of SR as a function of sub-aperture size and telescope diameter.

seeing (1.1 arcsec instead of 0.85 arcsec). Then we can verify that the effect of photon noise acts quite differently in the two sensors and the performance in detecting exoplanets will depend on the position in the field when AO errors due to photon noise dominate. More than a factor of 2 in intensity difference in the halo can be found in favour of a PS-based system in the range 0.1 to 0.7 arcsec, and up to a factor of 2 in favour of the SFSH sensor in the range 0.7 to 1.1 arcsec, for the conditions assumed here. The results may be somewhat different for lower flux and with read-out noise, but this is beyond the scope of this study.

4.1 Relative gain in sensitivity in the field

The theoretical PSDs of photon noise error propagation are shown in Fig. 4 for a SFSH sensor with the WCOG algorithm and a non-modulated PS. The latter was shown to be very similar to a direct phase sensor in terms of error propagation (Vérinaud 2004), so that this study can be applied to both the PS and Angel's Mach–Zehnder-based sensor. At first, we can notice that the SH error propagation increases dramatically when the sub-aperture size diminishes. This can be simply interpreted as the increase of the diffraction spot in the SH sub-apertures which induces more slope errors at a given flux. Secondly, the noise propagation for the SH sensor is a decreasing function of the spatial frequency, whereas it is increasing for the PS and thus the curves cross each other. The SR loss due to photon noise can be computed from the total residual phase variance obtained by integrating the PSDs over the range $[1/D, 1/(2d)]$. The relative gain in magnitude in terms of SR is thus a function of both D and d. The results are displayed in Fig. 5. It is interesting to note that for the PF configuration ($D = 8$ m, $d = 20$ cm) the gain provided by the PS, in case of no read-out noise, is thus only 0.4 mag. This gain can even be slightly negative for a small telescope, for example $D = 2$ m and $d = 20$ cm, since in this case the high-order error propagation for the PS will be larger than the low-order error in the SH sensor. For a 100-m ELT a gain with the PS of about 1 mag ($d = 20$ cm) is found. So taking into account the WCOG algorithm significantly reduces the overall gain in magnitude with respect to former studies (Ragazzoni & Farinato 1999; Esposito & Riccardi 2001; Carbillet et al. 2003; Vérinaud 2004). The SR, however, is not the only relevant parameter for high-contrast imaging. Indeed, as already noticed in Fig. 3, the performance depends on the location in the field. So it is more relevant to study the gain in magnitude as a function of the spatial frequency. In Fig. 6, we plot the ratio of the PSDs of Fig. 4 to get the relative gain directly. Hence we can see that the PS gain at low spatial frequencies can be up to

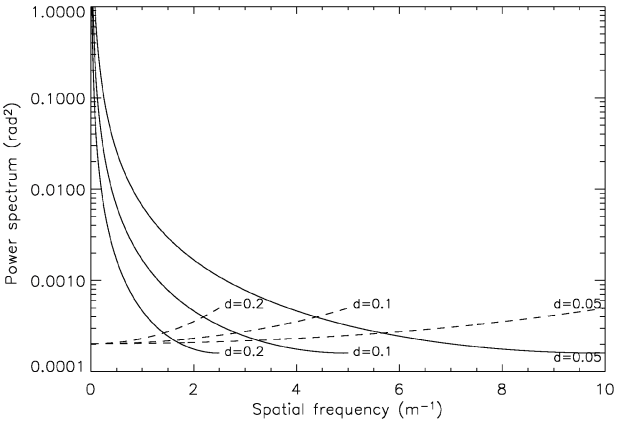

Figure 4. Theoretical PSDs of photon noise error propagation for the SH sensor (solid line) and for the PS (dashed line) for three different sub-aperture sizes (0.2, 0.1 and 0.05 m, from left to right).

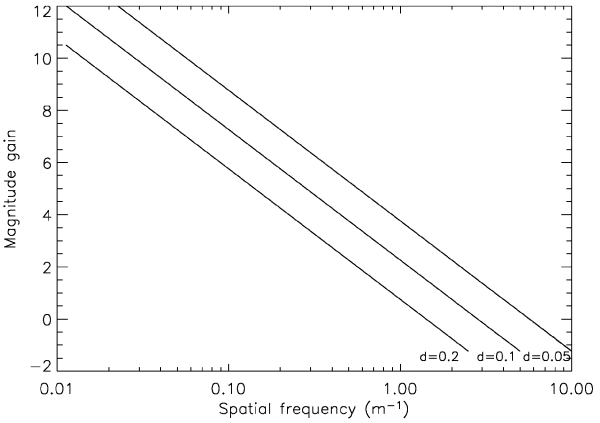

Figure 6. Gain in magnitude of the PS over the SH sensor as a function of spatial frequency.

several magnitudes (for example, about 6 mag at 0.1 m^{-1} for $d =$ 20 cm), and the smaller the spatial frequency the higher the gain provided by a phase-type sensor (or, more precisely, the higher the noise propagation for a slope sensor), whereas towards the highest frequencies the SH sensor can win up to 1 mag.

4.2 Implication for observation of exoplanets at visible light with ELTs

Visible light AO correction is an important challenge for ELTs, since it could permit very interesting science on exoplanets, like detection of gases (O_2, O_3), vegetation and other physical parameters (Schneider 2003). The characterization of exoplanets, and in particular the search for telluric planets with Earth-like features, will most probably require a large sample of targets. Hence it may be necessary to observe distant and faint stars with planets at small angular separation. The results of Section 4.1 have a direct impact on the detectability of planets in distant systems. We use, to compute residual haloes, the analytical models based on Rigaut et al. (1998) and Vérinaud (2004), taking into account the photon noise error propagation, servo-lag, and aliasing for the PS. For the study case that we propose, we assume that the maximum theoretical gain of the WCOG algorithm holds since high SR is obtained at the sensing wavelength. Let us consider a solar-type system with a host G2 V star of absolute magnitude $V = 4.7$ and an Earth-like planet at 1 au, 2×10^{-10} times fainter in visible light. We investigate the detectability of the planet with an AO-assisted 100-m ELT under mean to favourable atmospheric conditions (seeing: 0.7 arcsec; $\tau_0 = 3$ ms). To get a high SR (about 0.85 at high flux) in R, we consider a 15-cm actuator pitch (about 3×10^5 actuators) and a fast 4-kHz frame rate (to minimize servo-lag which is most probably the main error source for low-order residuals). For the detectors, we consider the same spectral bandwidth, 400 nm wide around a central 700-nm wavelength, for the sensing and the science instrument. Hence light is shared equally between them. The overall optical transmission of the telescope is 50 per cent.

We propose to investigate first the detectability of the planet against the halo (we suppose an efficient sparkle reduction technique is used, so speckle noise is neglected) with the full spectral bandwidth, with S/N = 3. Then we propose to consider also the possibility of obtaining spectral features of the planet, with S/N = 5 and a spectral resolution $R = 20$ that could permit the detection of atmospheric gases, for example (Schneider 2003). The integration time T needed to get a given S/N is $T \simeq (\mathrm{S/N})^2 \times N_*/N_\mathrm{p}^2$, where N_p is the number of photons per second coming from the planet (in an Airy disc weighted by the SR) and N_* is the number of photons in the halo at the location of the planet over a surface covered by an Airy disc. As an example, the AO residual haloes for SFSH-based and PS-based systems, when the stellar system is located at 50 pc, are represented in Fig. 7. In this case the magnitude of the star is $V = 8.2$, yielding 30 photons per sub-apertures and per sampling time. The SRs in R ($\mathrm{SR_{SH}} = 0.79$, $\mathrm{SR_{PS}} = 0.81$) are rather close, but the halo at the location of the Earth-like planet at 20 mas is 25 times brighter for the SFSH sensor than for the PS. Thus, there is the same ratio between the respective integration times needed to detect the planet ($T_\mathrm{SH} = 46.6$ h, $T_\mathrm{PS} = 1.65$ h) and for the spectral characterization ($T_\mathrm{SH} = 1400$ h, $T_\mathrm{PS} = 50$ h). Hence the planet could reasonably be detected and characterized with a PS but not with a SFSH sensor.

The general dependence of the required integration times on the distance of the stellar systems is given by Fig. 8. For our example, at up to 10 pc, the SFSH sensor and the PS are equivalent and permit us to get a spectrum of the planet in a few minutes. However, the advantage of the PS is clear for the observation of distant stars. We can see from Fig. 8 that, after 20 pc, if we fix the integration time, the PS permits the detection of the Earth-like planet in the considered stellar system up to twice as far away as with a SFSH sensor, which means the possibility of exploring a volume nearly an order of magnitude larger.

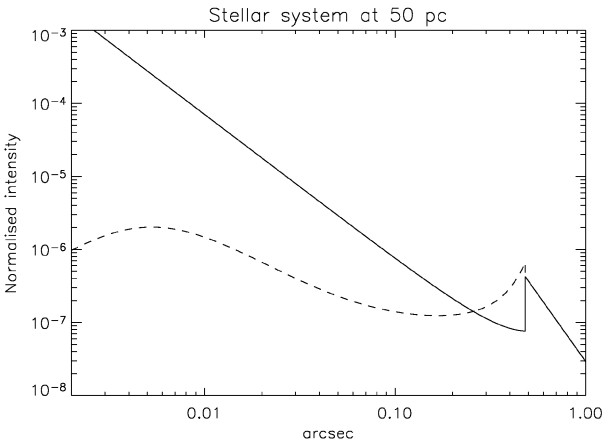

Figure 7. Residual halo in the R band for a SFSH-based system (solid line, SR = 0.79) and a PS-based system (dashed line, SR = 0.81) with a 15-cm actuator pitch on a 100-m telescope. The guide star V magnitude is 8.2, seeing = 0.7 arcsec, $\tau_0 = 3$ ms, frame rate = 4 kHz.

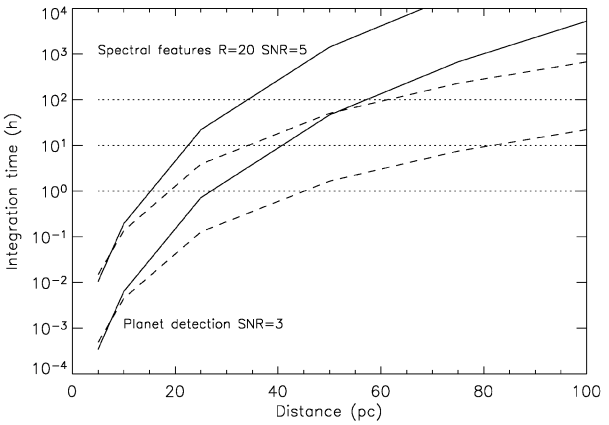

Figure 8. Detectability and spectral characterization of Earth-like planets as a function of the distance of the stellar system. Solid line: SFSH sensor; dashed line: PS.

5 CONCLUSIONS

In this Letter we have compared two different types of sensors, a wavefront slope sensor (the SFSH sensor) and a phase-type sensor (the PS) in the framework of high-contrast imaging. We took into account the latest developments for the SH sensor, like spatial filtering, permitting the attenuation of the aliasing error, and the WCOG algorithm which reduces the photon noise error on the centroiding. Our results show that the SFSH sensor can clearly compete with the PS at high flux. For photon noise limited AO corrections, we have shown that the intensity in the residual halo is a function of the position with respect to the star, so that the relative gain in sensitivity of one sensor with respect to the other, as a function of the spatial

frequency, is a much better indicator than the usual overall gain in magnitude in terms of SR. Hence a phase-type sensor is very well adapted for correcting the residual star halo near the centre, whereas a slope sensor shows better performance farther away. This behaviour can already be seen on an 8-m telescope, as we have shown by means of end-to-end simulations of a PF-type system in the *K* band. This is even more obvious for visible AO correction on ELTs. Indeed, we have shown that a tremendous gain can be provided by a phase-type sensor for the search for exoplanets at low angular separations, permitting, for example, a significant increase in the number of potential targets for Earth-like planet searches. Moreover, the combination with efficient speckle reduction techniques [see for example Codona & Angel (2004) and Guyon (2004)] will certainly be mandatory to reach or maybe improve the performance presented here even further.

From a technical point of view, control with Kalman filters Le Roux et al. (2004) could be very efficient when applied to phase-type sensors for better correction of servo-lag errors which dominate at low angular separations. We would like to emphasize also that the PS requires detectors with many fewer pixels than the SH sensor (unless a quad-cell SH sensor is used and the benefit of WCOG is lost), which is a very important advantage for ELTs and high-Strehl AO systems in general. We mention also that a high-order laboratory AO bench Hubin (2004), for characterizing jointly the PS and the SFSH sensor with its new features, will be developed at the European Southern Observatory in the framework of the OPTICON Joint Research Activity funded by the European Commission, in the sixth framework programme.

Finally, we mention the possibility of improving the performance of a slope sensor for high-contrast imaging by using a hierarchical SH sensor Le Roux et al. (2005) that could be optimized as a function of the angular separation where a planet could be searched for. This multi-stage concept for wavefront sensing could even be generalized by considering the combination of sensors with different properties (pyramid with Shack–Hartmann sensor or even pyramid with curvature sensor) in order to obtain a more uniform correction around the star.

ACKNOWLEDGMENTS

The authors acknowledge the anonymous referee for very constructive criticism of the original manuscript. This work was supported by the European Community within the framework of the Research and Training Network (RTN) 'Adaptive Optics for Extremely Large Telescopes' with contract No. HPRN-CT-2000-00147.

REFERENCES

Angel R., 1994, Nat, 368, 203
Berton A. et al., 2004, in Bonaccini D., Ellerbroek B. L., Ragazzoni R., eds, Proc. SPIE Vol. 5490, Advancements in Adaptive Optics. SPIE, Bellingham, WA, p. 672
Beuzit J. L. et al., 2004, SF2A-2004, Semaine de l'Astrophysique Francaise. EdP-Science, Gif-sur-Yvette
Carbillet M., Vérinaud C., Esposito S., Riccardi A., Puglisi A., Femenía B., Fini L., 2003, in Wizinowich P. L., Bonaccini D., eds, Proc. SPIE Vol. 4839, Adaptive Optical System Technologies. SPIE, Bellingham, p. 131
Codona J. L., Angel R., 2004, ApJ, 604, L117
Esposito S., Riccardi A., 2001, A&A, 369, L9
Fusco T., Nicolle M., Michau V., Rousset G., Beuzi J. L., Mouillet D., 2004, in Bonaccini D., Ellerbroek B. L., Ragazzoni R., eds, Proc. SPIE Vol. 5490, Advancements in Adaptive Optics. SPIE, Bellingham, p. 1155
Guyon O., 2004, ApJ, 615, 562
Hubin N., 2004, in Bonaccini D., Ellerbroek B. L., Ragazzoni R., eds, Proc. SPIE Vol. 5490, Advancements in Adaptive Optics. SPIE, Bellingham, p. 195
Jolissaint L., Véran J. P., 2002, in Vernet E., Ragazzoni R., Esposito S., eds, ESO Conf. and Workshop Proc. 58, Beyond Conventional Adaptive Optics. ESO, Garching, p. 201
Korkiakoski V., Vérinaud C., Le Louarn M., 2004, in Bonaccini D., Ellerbroek B. L., Ragazzoni R., eds, Proc. SPIE Vol. 5490, Advancements in Adaptive Optics. SPIE, Bellingham, p. 695
Le Louarn M., Braud J., Fedrigo E., Korkiakoski V., Vérinaud C., 2004, in Bonaccini D., Ellerbroek B. L., Ragazzoni R., eds, Proc. SPIE Vol. 5490, Advancements in Adaptive Optics. SPIE, Bellingham, p. 705
Le Roux B., Conan J. M., Kulcsar C., Raynaud H. F., Mugnier L. M., Fusco T., 2004, J. Opt. Soc. Am. A, 21, 7
Le Roux B. et al., 2005, Appl. Optics, 44, in press
Nicolle M., Fusco T., Rousset G., Michau V., 2004, Opt. Lett., 23, 2743
Poyneer L. A., Machintosh B., 2004, J. Opt. Soc. Am. A, 21, 810
Ragazzoni R., 1996, J. Mod. Opt., 43, 289
Ragazzoni R., Farinato J., 1999 A&A, 350, L23
Rigaut F., Véran J. P., Lai O., 1998, in Proc. SPIE Vol. 3353, Adaptive Optical System Technologies. SPIE, Bellingham, p. 1038
Schneider J., 2003, EAS Publ. Ser., Vol. 8, Astronomy with High Contrast Imaging, p. 1
Vérinaud C., 2004, Opt. Commun., 233, 27

This paper has been typeset from a TEX/LATEX file prepared by the author.